Article
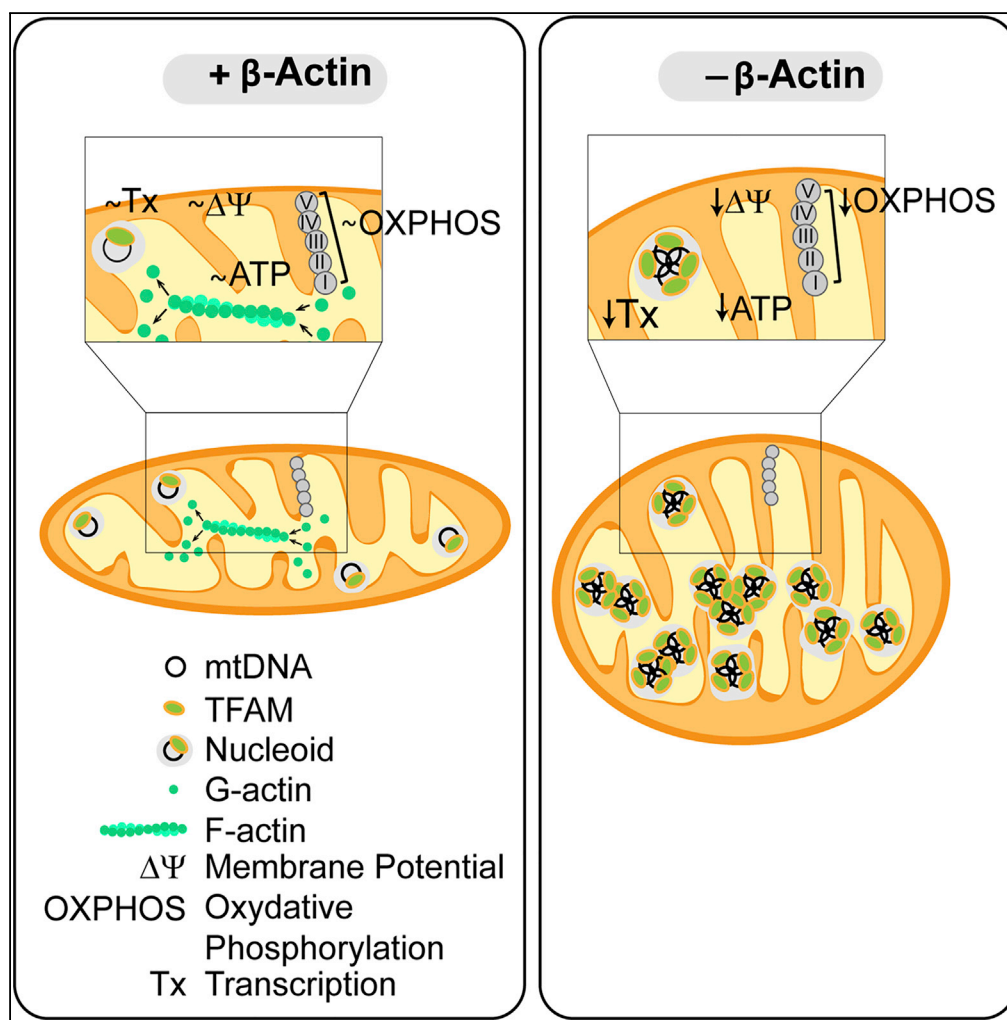
In Mitochondria β-Actin Regulates mtDNA Transcription and Is Required for Mitochondrial Quality Control

Xin Xie, Tomas Venit, Nizar Drou, Piergiorgio Percipalle

pp69@nyu.edu

HIGHLIGHTS

Maintenance of mitochondrial membrane potential (MMP) requires β-actin

MMP defects are due to impaired mtDNA and nucleus-encoded OXPHOS gene transcription

Loss of mitochondrial β-actin-containing structures leads to nucleoid aggregation

Mitochondria-targeted β-actin rescued mtDNA transcription and MMP

Article

In Mitochondria β-Actin Regulates mtDNA Transcription and Is Required for Mitochondrial Quality Control

Xin Xie,[1] Tomas Venit,[1] Nizar Drou,[2] and Piergiorgio Percipalle[1,3,4,*]

SUMMARY

In eukaryotic cells, actin regulates both cytoplasmic and nuclear functions. However, whether actin-based structures are present in the mitochondria and are involved in mitochondrial functions has not been investigated. Here, using wild-type β-actin +/+ and knockout (KO) β-actin −/− mouse embryonic fibroblasts we show evidence for the defect in maintaining mitochondrial membrane potential (MMP) in β-actin-null cells. MMP defects were associated with impaired mitochondrial DNA (mtDNA) transcription and nuclear oxidative phosphorylation (OXPHOS) gene expression. Using super-resolution microscopy we provided direct evidence on the presence of β-actin-containing structures inside mitochondria. Large aggregates of TFAM-stained nucleoids were observed in bulb-shaped mitochondria in KO cells, suggesting defects in mitochondrial nucleoid segregation without β-actin. The observation that mitochondria-targeted β-actin rescued mtDNA transcription and MMP suggests an indispensable functional role of a mitochondrial β-actin pool necessary for mitochondrial quality control.

INTRODUCTION

In the cytoplasm actin is known to regulate cell morphology, movement, and organelle dynamics and function (Dominguez and Holmes, 2011). Specific interactions of cytosolic actin with mitochondria are known to mediate fission of mitochondrial networks and mitochondrial transport, contributing to cellular distribution of mitochondria (Boldogh and Pon, 2006; Senning and Marcus, 2010). Although the exact mechanism remains to be fully unveiled, cytosolic actin is also involved in mitochondria-dependent apoptosis (Gourlay and Ayscough, 2005). Evidence also suggests that actin and some actin-associated proteins such as myosin are involved in mitochondrial function through specific association with mitochondrial DNA (mtDNA) (Reyes et al., 2011).

Functional association of actin with DNA has been described in both prokaryotes and eukaryotes (Moller-Jensen et al., 2002; Visa and Percipalle, 2010). In the eukaryotic cell nucleus, actin interacts with active genes and controls transcription by all three eukaryotic nuclear RNA polymerases (Visa and Percipalle, 2010). At the genomic level, β-actin regulates chromatin distribution and deposition of epigenetic marks, leading to activation or repression of gene programs, and affects cellular identity (Xie et al., 2018). In rod-shaped bacteria, actin-like proteins play an important role in genomic and plasmid DNA segregation (Kruse and Gerdes, 2005; Moller-Jensen et al., 2002). Given their circular genome and the fact that mtDNA maintenance and replication are independently performed, it is possible that actin-based mechanisms are fundamental for mtDNA segregation. Indeed, β-actin and myosin were found to associate with mitochondrial nucleoids, and a pool of β-actin resistant to protease digestion was identified in isolated mitochondria (Reyes et al., 2011), suggesting that β-actin is localized in mitochondria. However, how β-actin is organized inside mitochondria and whether mitochondrial β-actin plays a functional role in mitochondrial quality control is unknown.

In this study, we analyzed embryonic fibroblasts from wild-type (WT) β-actin +/+ mice and knockout (KO) β-actin −/− mice (Tondeleir et al., 2012). When comparing KO cells lacking both functional β-actin alleles with WT cells, we found a severe defect in maintaining mitochondrial membrane potential (MMP). This defect can be attributed to impaired mtDNA transcription and down-regulation of nucleus-encoded oxidative phosphorylation (OXPHOS) genes. Using super-resolution microscopy, we observed β-actin-containing structures inside mitochondria, which seem to be connected to the cytosolic counterparts. In the absence of β-actin, mitochondrial nucleoids tend to form large aggregates in bulbous mitochondria. Together with the significantly increased mtDNA copy number in KO cells, our finding suggests that

[1]Science Division, Biology Program, New York University Abu Dhabi (NYUAD), P.O. Box 129188, Abu Dhabi, United Arab Emirates

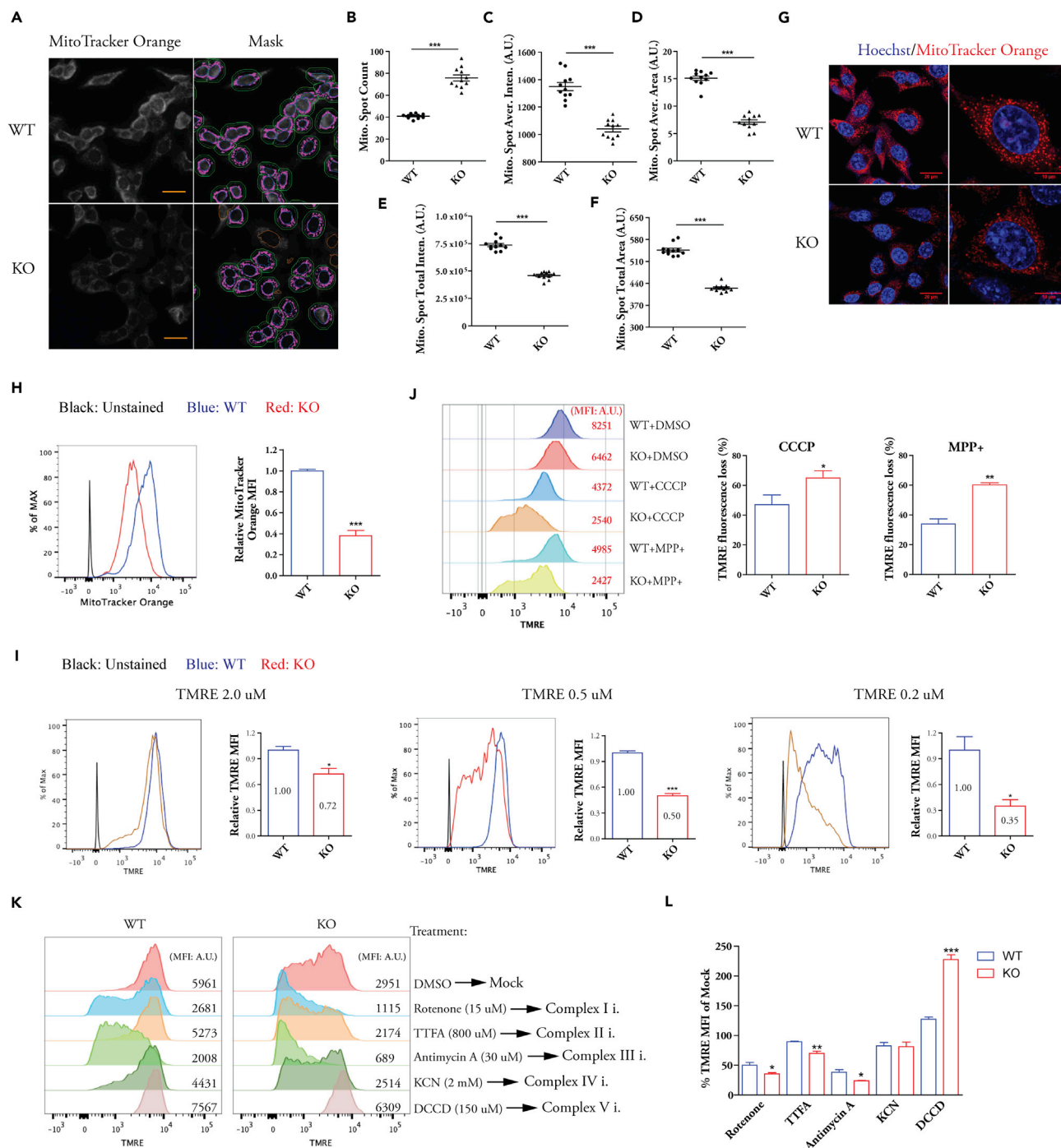[2]NYU Abu Dhabi Center for Genomics and Systems Biology, Abu Dhabi, UAE

[3]Department of Molecular Biosciences, The Wenner-Gren Institute, Stockholm University, S-106 91 Stockholm, Sweden

[4]Lead Contact

*Correspondence: pp69@nyu.edu

Figure 1. Impaired MMP and Hypersensitivity to Mitochondrial Stress in β-Actin Knockouts

(A) WT and KO MEFs stained with MitoTracker Orange were analyzed using a high-content phenotypic platform. Right panel shows the mask of detected staining signal. The green color delineates the simulated cytoplasmic boundary of individual cells, and the inner blue circle defines the nuclear region of stained DNA. The magenta color displays the detected MitoTracker Orange staining within the simulated cytoplasm. Scale bar, 20 μm.

(B–F) Quantification of MitoTracker Orange signal in single cells. (B) Spot count; (C) spot average intensity; (D) spot average area; (E) spot total intensity; and (F) spot total area. Each data point represents mean of at least 500 single cells in one biological replicate, representative of three independent experiments.

(G) Confocal image of MEFs stained with MitoTracker Orange.

(H) FACS analysis of MEFs stained with MitoTracker Orange. Data are the summary of the mean fluorescence intensity (MFI), n = 3 independent experiments.

(I) FACS analysis of MEFs stained with decreasing concentrations of TMRE. The relative TMRE MFI of WT cells and KO cells at each condition was calculated; n = 3 independent experiments.

Figure 1. Continued

(J) FACS analysis of MMP change after MPP+ (2 mM) and CCCP (30 μM) treatment by TMRE staining; n = 3 independent experiments. DMSO treatment was used as mock control to calculate the % TMRE fluorescence loss. DMSO, dimethyl sulfoxide.

(K and L) MEFs were treated with selective inhibitors of complex I to V. MMP changes were analyzed by TMRE staining (K). Mean TMRE fluorescence intensity change relative to mock is shown in (L); n = 3 biological replicates.

Data are presented as mean ± SEM *p ≤ 0.05, **p ≤ 0.01, ***p ≤ 0.001. Student's t test. SEM, standard error of the mean.

See also Figure S1 and Videos S1, S2, and S3.

mitochondrial nucleoids are defective in segregation after mtDNA replication. Importantly, mitochondria-targeted β-actin rescued mtDNA transcription and MMP when constitutively re-introduced into β-actin-null cells. Overall, our study provides direct evidence on the presence of β-actin in mitochondria and unveils a yet unknown role of the mitochondrial pool of β-actin in mitochondrial quality control.

RESULTS

Defects of Mitochondrial Membrane Potential (MMP) Maintenance in Cells Lacking β-Actin

We used high-content screening platform to analyze the mitochondrial features of mouse embryonic fibroblasts from WT (β-actin +/+) and KO (β-actin −/−) embryos (Tondeleir et al., 2012). Cells stained by a MitoTracker Orange dye, which accumulates in the mitochondria depending on the membrane potential and is well retained after fixation, were subjected to quantitative analysis of stained mitochondrial spots (MitoTracker Orange-positive staining) in single cells (Figure 1A). We found that, in comparison with WT cells, there were more stained spots in the cytoplasm of KO cells (Figure 1B). However, the average spot intensity is significantly lower and the average spot area is smaller in KO cells (Figures 1C and 1D). The value of total spot area and intensity in each cell was also significantly lower in KO cells on average (Figures 1E and 1F). These data indicate that, in the absence of β-actin, smaller mitochondrial regions could maintain membrane potential, leading to an overall lower MMP in KO cells. Confocal images essentially confirmed the results from the high-content screening (Figure 1G). Fluorescence-activated cell sorting (FACS) analysis demonstrated that KO cells lost more than 50% MMP based on MitoTracker Orange staining (Figure 1H). The significant loss of MMP was not observed in heterozygous cells with only one functional β-actin allele (Figure S1A). Therefore, the severe MMP loss only happens in the absence of two functional β-actin alleles.

We further used tetramethylrhodamine ethyl ester (TMRE) that dynamically accumulates or associates with mitochondria depending on MMP to stain living cells. The staining intensity declined with decreasing concentrations of TMRE applied to both WT and KO cells. However, at all concentrations, KO cells displayed significantly lower TMRE staining intensity compared with WT cells (Figure 1I). Remarkably, the difference of TMRE intensity between WT and KO cells became larger at lower concentration (Figure 1I). Therefore, KO cells displayed defects in accumulating TMRE especially at low concentration, indicating impaired ability to maintain the dynamic MMP.

Increased Sensitivity to Mitochondrial Stress and Altered Mitochondrial Morphology in the Absence of β-Actin

We next investigated MMP changes under mitochondrial stress induced by MPP+ (1-methyl-4-phenylpyridinium, a specific complex I inhibitor) and CCCP (Carbonyl cyanide m-chlorophenyl hydrazone, a mitochondrial uncoupler) (Qi et al., 2013). MPP+ and CCCP treatment reduced TMRE staining in both WT and KO cells (Figure 1J, left panel). However, KO cells lost more MMP (TMRE intensity) after MPP+ and CCCP stress treatment (Figure 1J, right panel). Consistently, live cell images demonstrated that KO cells are very sensitive to CCCP stress and display rapid cell shrinkage after CCCP addition (Video S1). Furthermore, after mitochondrial membrane depolarization by high concentration of CCCP, KO cells also showed an impaired recovery of MMP compared with WT cells (Figures S1B and S1C). Together, these data show that cells without β-actin are more sensitive to mitochondrial stress caused by MMP impairment, which in turn is linked to an intrinsic defect in MMP maintenance.

We further applied selective inhibitors of electron transport chain complexes and found that KO cells are more sensitive to the activity inhibition of complexes I, II, and III, as manifested by the greater loss of MMP when compared with WT cells (Figures 1K and 1L). Importantly, inhibition of complex V (ATP synthase) by DCCD (N,N-dicyclohexylcarbodiimide) led to MMP increase in both WT and KO cells; however, the degree of MMP increase is much higher in KO cells (Figure 1L). Since DCCD inhibits proton translocation in ATP synthase (complex V) without significant effect on electron transfer activity (Clejan et al., 1984; Toei and
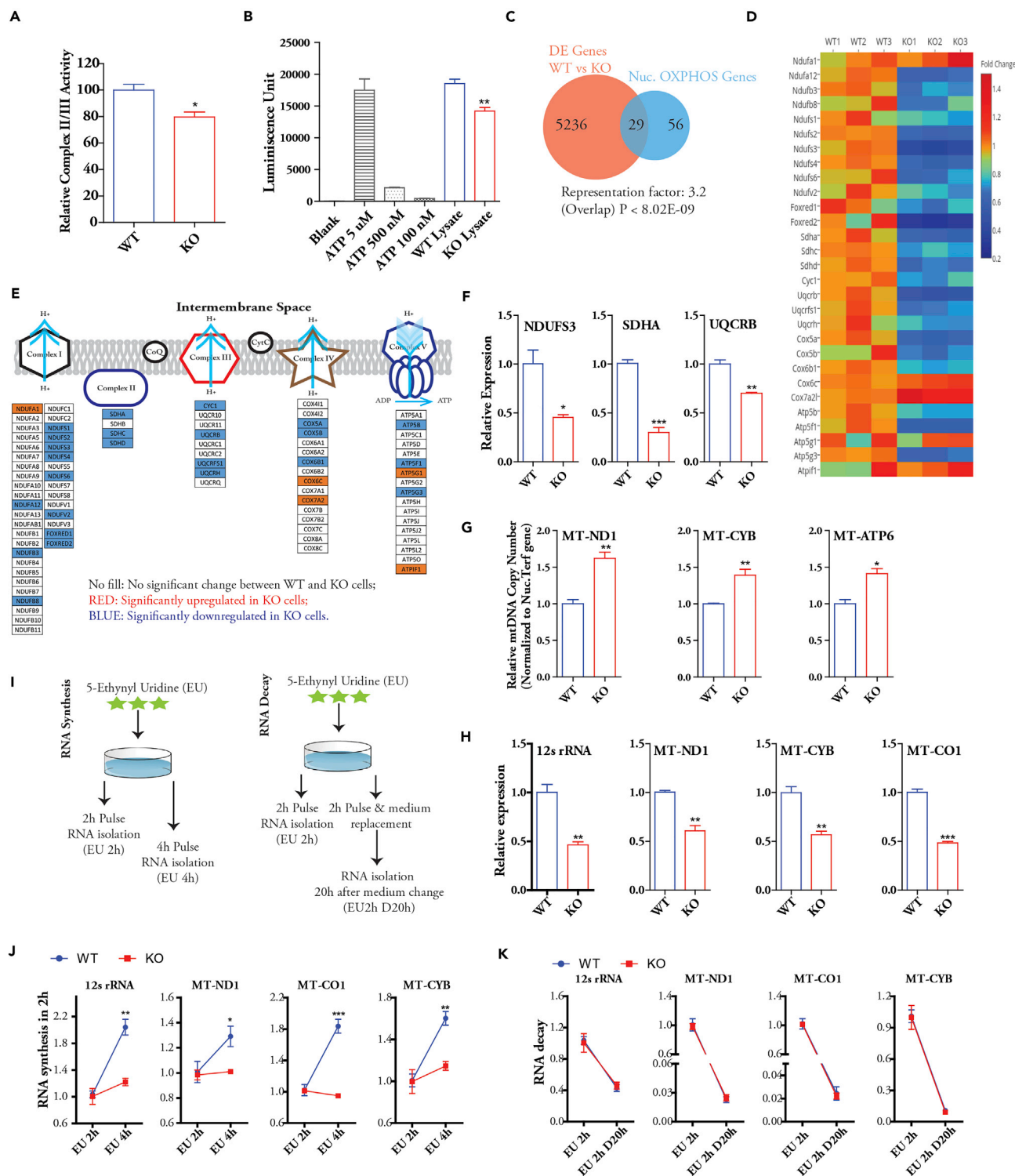
Figure 2. OXPHOS Defects Are Linked to Impaired mtDNA and Nuclear OXPHOS Gene Expression in β-Actin Knockouts

(A) Mito complex II/III activity assay of isolated mitochondria; n = 3 independent experiments.

(B) Cellular ATP level determination; n = 3 independent experiments.

(C) Venn diagram showing significant overlap of differentially expressed genes in WT versus KO MEFs and OXPHOS genes encoded by nucleus: Fisher's exact test.

Figure 2. *Continued*

(D) Relative expression levels of nuclear OXPHOS genes differentially expressed between WT and KO cells by RNA-seq. The mean value of WT samples was set as 1.

(E) Distribution of differentially expressed nuclear OXPHOS genes.

(F) Quantification of mRNA level of Ndufs3, Sdha, and Uqcrb genes by qPCR; n = 3 biological replicates.

(G) mtDNA level determination using MT-ND1, MT-CYB, and MT-ATP6 genes by qPCR; n = 3 independent experiments.

(H) Transcript level of 12s rRNA, MT-ND1, MT-CYB, and MT-CO1 genes by qPCR; n = 3 independent experiments.

(I–K) Schematics of RNA synthesis and RNA decay experiments are shown in (I). qPCR analysis of mt-RNA synthesis (J) and decay (K); n = 3 biological replicates.

Data are presented as mean ± SEM *p ≤ 0.05, **p ≤ 0.01, ***p ≤ 0.001. Student's t-test. SEM, standard error of the mean.

See also Figure S2.

Noji, 2013), our results suggest that the mitochondrial intermembrane space has more unused capacity for proton storage in KO cells than in WT cells when ATP synthase is blocked. Therefore, the lower MMP in KO cells is due to the lack of proton accumulation instead of the lack of proton storage capacity of mitochondria.

Several studies showed that MMP alterations could lead to changes in mitochondrial morphology (Leonard et al., 2015; Safiulina et al., 2006). We therefore investigated mitochondrial morphology in live cells using MitoTracker Deep Red, which accumulates in mitochondria regardless of the MMP. As expected, we found that the majority of WT cells showed a network of thin filamentous mitochondria. In contrast, KO cells exhibited swollen mitochondria with bulbous shape (Figure S1D and Video S2). Since mitochondria swelling and increase in volume are associated with loss of MMP (Leonard et al., 2015; Safiulina et al., 2006), the observed mitochondrial morphology in KO cells is likely to be caused by the severely impaired MMP. We further tested whether reducing MMP in WT cells leads to similar morphological changes. In the presence of MPP+, we observed the gradual formation of bulbous mitochondria after 30-min treatment in WT cells (Figure S1E). Live cell images showed that the initially rod-shaped mitochondria gradually shortened along the length and became spherical (Video S3). The level of bulbous mitochondria was also found to increase in KO cells after MPP+ treatment (Video S3). Collectively, our data show that β-actin is indispensable in controlling MMP and the morphology of mitochondria.

In β-Actin Knockouts, Impaired Transcription of OXPHOS Genes from mtDNA and Nucleus Is Coupled to Decreased OXPHOS Activity

MMP is maintained by the activity of electron transport chain complexes during OXPHOS (Dzbek and Korzeniewski, 2008). To study the electron transport activity in the absence of β-actin, we isolated mitochondria from WT and KO cells and compared the complex II/III activity. Mitochondria from KO cells showed a significantly lower level of complex II/III activity (Figure 2A). Consistently, KO cells produced an overall lower cellular ATP level than WT cells (Figure 2B), altogether demonstrating an impaired OXPHOS activity in the absence of β-actin. We then analyzed the relative expression levels of nuclear OXPHOS genes using a recently published RNA-seq dataset (Xie et al., 2018). Remarkably, nuclear OXPHOS genes were found to be significantly overrepresented in the differentially expressed (DE) genes between WT and KO cells (Figure 2C). These results imply that impaired OXPHOS activity in KO cells is a direct consequence of altered OXPHOS gene expression. Consistent with impaired MMP, the majority of DE OXPHOS genes showed down-regulation in KO cells (Figure 2D). These down-regulated genes mainly encode components of complexes I, II, and III in the electron transport chain (Figure 2E). We verified the lower expression of *Ndufs3*, *Sdha,* and *Uqcrb* in KO cells by quantitative polymerase chain reaction (qPCR) (Figure 2F). The overall down-regulation tendency of OXPHOS genes is consistent with the previous finding that nuclear components of OXPHOS are transcriptionally co-regulated (van Waveren and Moraes, 2008).

Essential components of electron transport complexes are also encoded by the mitochondrial genome. There is evidence that β-actin and myosin play a role in mtDNA topology and copy number maintenance (Reyes et al., 2011). However, how the mtDNA copy number and mtDNA transcription are potentially regulated by β-actin is not known. We therefore analyzed the status of mtDNA copy number and its transcript in KO cells. We found that in the absence of β-actin there is an increase in mtDNA copy number, as revealed by the quantification of a subset of mtDNA loci (Figure 2G). Furthermore, total DNA sequencing also revealed an overall higher mtDNA level across the mtDNA genome in KO cells (Figure S2A). However, the expression of transcripts from mtDNA was significantly reduced in KO cells (Figure 2H). The decreased level of mtDNA transcript may be due to decreased RNA synthesis or increased RNA degradation. To
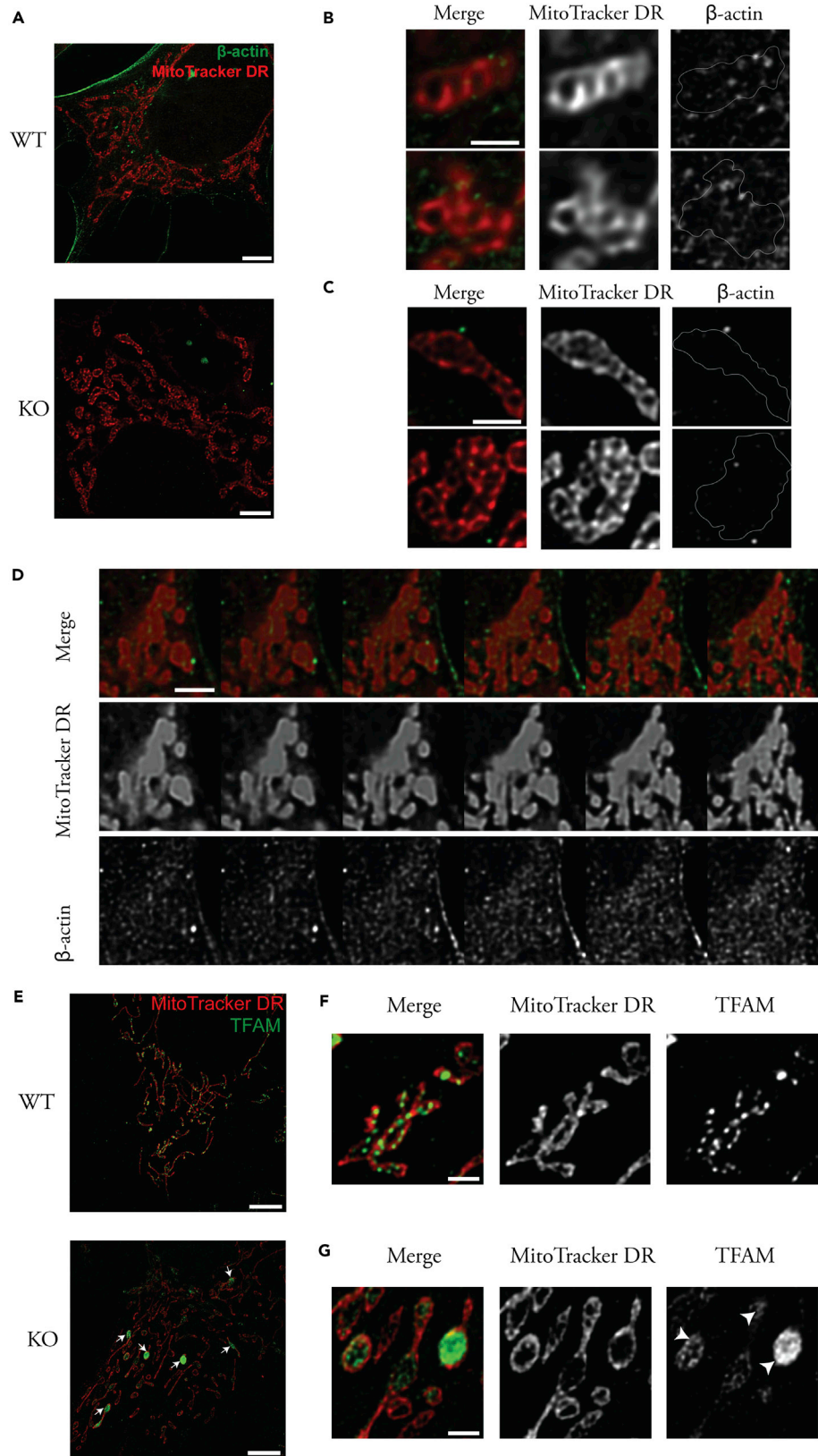
Figure 3. A Pool of β-Actin Resides in Mitochondria, Without Which TFAM-Stained Nucleoids Tend to Form Large Aggregates

WT and KO MEFs were stained with MitoTracker Deep Red (red) and a β-actin-specific antibody (green) or anti-TFAM antibody (green) and visualized by STED microscope.

(A) Comparison of β-actin staining and its distribution between WT and KO cells. Scale bar, 5 μm.

(B and C) STED microscope image insets selected from WT cell (B) and KO cell (C). Gray lines represents the boundary of mitochondria in the β-actin insets; scale bar, 1 μm.

(D) Montage of six consecutive z stack confocal images in WT cells, moving 250 nm in each step. Scale bar, 2 μm.

(E) STED microscope image of MitoTracker Deep Red (red) and anti-TFAM antibody (green) staining in WT and KO cells; scale bar, 5 μm. Arrows point to examples of enlarged mitochondria.

(F and G) STED microscope image insets selected from WT cell (F) and KO cell (G); scale bar, 1 μm; arrowheads in (G) indicate TFAM-based nucleoid aggregates.

See also Figures S3 and S4.

distinguish between the two possibilities, newly synthesized RNA was labeled with 5-ethynyl uridine to monitor the rate of RNA synthesis and decay (Figure 2I, see also Transparent Methods). For RNA synthesis, we pulse-labeled the cells for 2 and 4 hr to quantify the relative RNA changes within 2-hr intervals (Figure 2I, left panel). For the RNA decay experiment, labeled cells were cultured in fresh medium to determine the remaining amount of labeled RNA after 20 hr (Figure 2I, right panel). We observed that the absence of β-actin in KO cells leads to impaired RNA synthesis without affecting the RNA decay (Figures 2J and 2K). Altogether, our data demonstrate that in the absence of β-actin, nuclear OXPHOS genes are down-regulated and mtDNA transcription is impaired, suggesting that nuclear and mitochondrial genomes are coordinated to balance the expression of OXPHOS components. The correlation between nuclear and mitochondrial expression of OXPHOS subunits has also been reported in previous studies (Gagnon et al., 1991; Murdock et al., 1999). Consistent with reduced expression of OXPHOS components, KO cells displayed an overall lower mitochondrial mass as assessed by MitoTracker Deep Red staining (Figure S2B) (Schieke et al., 2006).

A Pool of β-Actin Is Located Inside Mitochondria and Mitochondrial Nucleoids form Large Aggregates in the Absence of β-Actin

As both nuclear OXPHOS genes and mtDNA transcription are affected without β-actin, a key question is whether β-actin functions primarily in the cytoplasm or in the nucleus to control OXPHOS genes. We first used the recently published plasmids containing green fluorescent protein (GFP)-β-actin and GFP-nuclear localization signal (NLS)-β-actin (Sharili et al., 2016) and transiently expressed them in KO cells. As expected, the GFP-β-actin was mainly in the cytoplasm and the NLS-β-actin was enriched in the nucleus (Figure S3A). However, neither β-actin nor NLS-β-actin showed rescue effects on the MMP in KO cells (Figures S3B–S3D). The level of overexpressed exogenous β-actin in KO cells is much lower than that of the endogenous β-actin in WT cells (Figure S3E). Nevertheless, the fact that nucleus-targeted β-actin failed to rescue MMP prompted us to investigate a potential role of β-actin inside the mitochondria.

A previous report showed that mtDNA associates with β-actin and myosin, and a pool of β-actin in isolated mitochondria seems to be resistant to protease digestion (Reyes et al., 2011; Wang and Bogenhagen, 2006). However, there is no direct evidence showing that β-actin-containing structures reside in the mitochondria of mammalian cells. To demonstrate the localization of β-actin inside mitochondria, we co-stained WT and KO MEFs with MitoTracker Deep Red and β-actin-specific antibody, and visualized the cells by stimulated emission depletion (STED) microscopy. Consistent with a previous study (Shestakova et al., 2001), β-actin was enriched at the plasma membrane in WT cells, with weaker staining of β-actin-containing structures in the cytoplasm (Figure 3A). The absence of β-actin staining in KO cells demonstrate the specificity of the β-actin antibody (Figure 3A). Detailed analysis showed that β-actin-containing structures were widely distributed in both the cytoplasm and mitochondria in WT cells, which are absent in KO cells (Figures 3B and 3C). It is noteworthy that β-actin seems to form an interconnected network in both the cytoplasm and mitochondria of WT cells (Figure 3B). z Stack confocal images also showed that β-actin is localized around as well as inside the mitochondria in WT cells (Figure 3D). Together, these results provide strong evidence that β-actin resides in the mitochondria and seems to be connected with cytoplasmic counterparts.

We also stained WT cell with phalloidin, which selectively binds to polymerized F-actin. The strongest phalloidin staining localized at the cell periphery or the actin fibers inside cytoplasm (Figure S4A). Phalloidin staining was observed around the mitochondria, and a relatively weak and network-like phalloidin staining
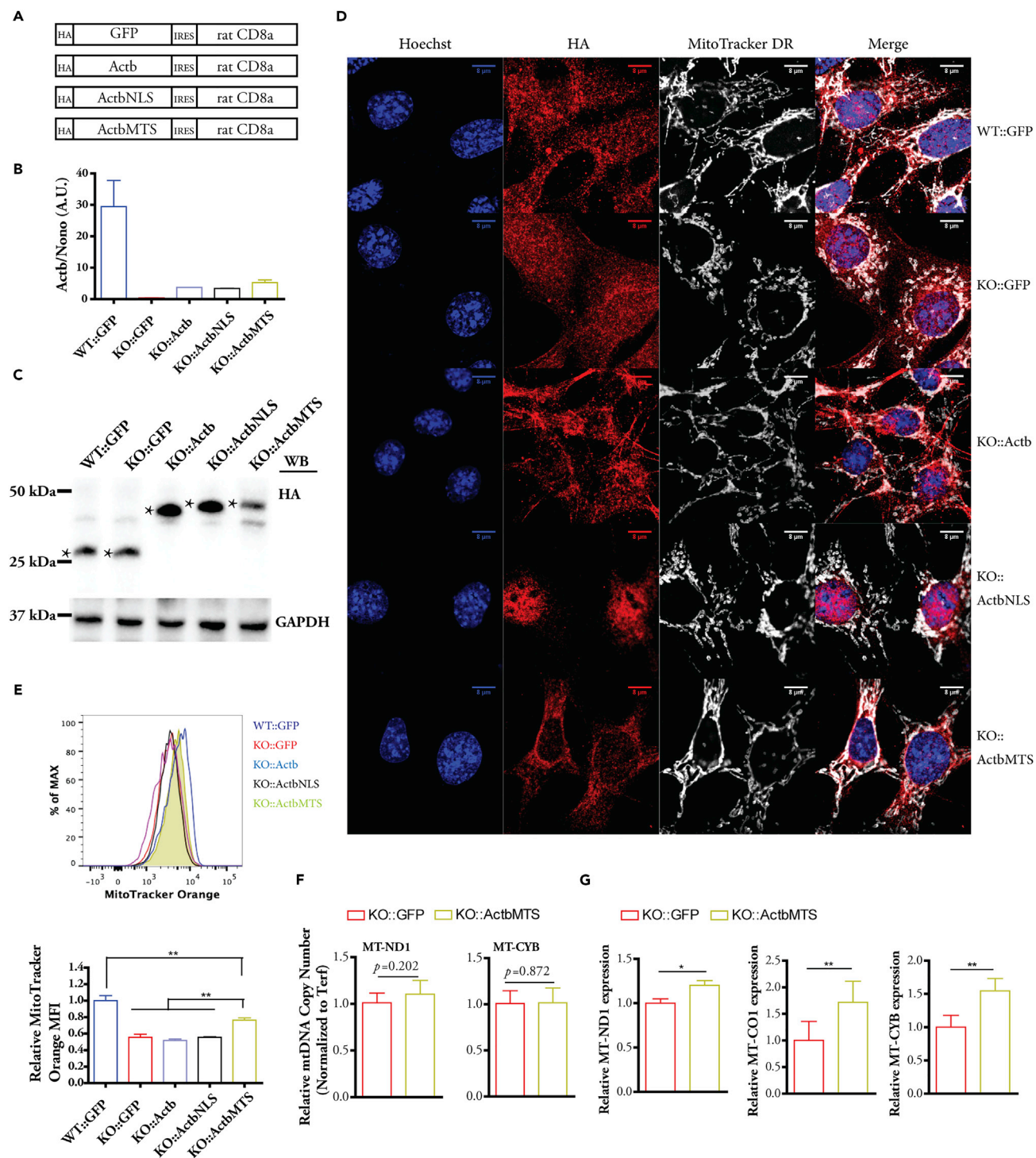
Figure 4. Mitochondria-Targeted β-Actin but Not Nucleus-Targeted β-Actin Shows Rescue Effect on MMP

(A) Schematics of retroviral constructs used for re-introducing GFP, β-actin (Actb), β-actin with NLS (ActbNLS), and β-actin with MTS (ActbMTS) into KO (β-actin−/−) MEFs.

(B) qPCR quantification of relative expression level of β-actin mRNA. WT::GFP represents WT cells transduced with retrovirus carrying GFP; n = 3 biological replicates.

(C) Western blot of protein levels of HA-tagged GFP and β-actin. The HA-GFP (first two lanes), HA-tagged β-actin, β-actin with NLS, and β-actin with MTS are indicated by asterisk, with expected molecular weights.

Figure 4. *Continued*

(D) Confocal images of localization of HA-tagged GFP, β-actin, β-actin with NLS, and β-actin with MTS. Scale bar, 8 μm.

(E) FACS analysis of MMP stained by MitoTracker Orange; n = 4 independent experiments. One-way analysis of variance (ANOVA) with Tukey's post hoc test: mean $\pm$ SEM, **p $\leq$ 0.01). SEM, standard error of the mean.

(F) mtDNA level comparison between KO::GFP and KO::ActbMTS cells; n = 3 biological replicates, Student's t test.

(G) Transcript level of MT-ND1, MT-CYB, and MT-CO1 between KO::GFP and KO::ActbMTS cells; n = 3 independent experiments; Student's t test: mean $\pm$ SEM *p $\leq$ 0.05, **p $\leq$ 0.01.

See also Figure S5.

was also seen inside the mitochondria and in the cytoplasm (Figure S4B). The data therefore suggest that, in addition to forming strong actin fibers, polymerized actins form network-like structures both around and inside the mitochondria. However, it should be pointed out that phalloidin stains F-actins formed by different actin isoforms.

The presence of β-actin network inside mitochondria resembles actin-like cytoskeleton in bacteria, which is essential for plasmid partitioning (Carballido-Lopez, 2006; Kruse and Gerdes, 2005). We then analyzed the nucleoid based on mitochondrial transcription factor A (TFAM) staining, which is the main factor for mtDNA packaging (Kukat and Larsson, 2013). In WT mitochondria, we observed a relatively uniform size of TFAM-based nucleoid, which is efficiently distributed along the tubular mitochondria (Figures 3E and 3F). This is consistent with recent studies in which mammalian mitochondrial nucleoids show uniform size and frequently contain a single mtDNA compacted by TFAM (Kukat et al., 2011, 2015). However, we observed that TFAM-containing nucleoids tend to form clustered aggregates in bulbous mitochondria in β-actin-null cells (Figures 3E and 3G, see arrows). We wonder whether this topological change affects TFAM binding on mtDNA. TFAM chromatin immunoprecipitation sequencing (ChIP-seq) analysis on mitochondrial genome shows that TFAM binding was evenly distributed across the whole mtDNA in both WT and KO cells (Figure S4C). Together, these data suggest that β-actin-containing structure is involved in the segregation and distribution of mitochondrial nucleoids, but is not required for the binding of TFAM on mtDNA.

Mitochondria-Targeted β-Actin Partially Rescues MMP and Increases mtDNA Transcription

To demonstrate a functional role for the mitochondrial β-actin pool, we used a retroviral system to re-introduce into KO cells WT β-actin, β-actin with NLS, and β-actin with cytochrome c oxidase subunit 4 (COX4) mitochondria-targeting sequence (MTS) (Chatterjee et al., 2016). A retroviral system with rat CD8a extracellular domain as a transduction marker was used to generate cells stably expressing different constructs (Xie et al., 2015). A GFP construct was used as control for viral transduction (Figures 4A and S5A). Cells expressing the transduction marker rCD8a (cell surface marker used for sorting) were sorted by FACS, and about 90% of cells stably expressed rCD8a marker after expansion (Figure S5B, KO::Actb: KO cells transduced with virus carrying *Actb* gene). The re-introduced Actb, ActbNLS, and ActbMTS constructs in KO cells showed comparable messenger RNA (mRNA) expression levels, although at much lower levels when compared with endogenous β-actin in WT cells (Figure 4B). However, the ActbMTS displayed a lower protein level when compared with Actb and ActbNLS constructs (Figure 4C). This may be due to the impaired stability caused by the folding and refolding process during mitochondrial import through the double membrane (Dudek et al., 2013), or due to the mitochondrial protein quality control by proteases (Hamon et al., 2015).

The low expression of re-introduced β-actin was not clearly detected by anti β-actin antibody (data not shown). Instead, we stained the cells with high-affinity anti-hemagglutinin (HA) antibody and observed differential localization patterns (Figure 4D). As expected, we observed actin fiber formation in the cytoplasm of KO::Actb cells and the enrichment of β-actin in the nucleus of KO::ActbNLS cells (Figure 4D). β-Actin with MTS seems to be preferentially localized to the mitochondria, especially those located around the nucleus (Figure 4D). Super-resolution images demonstrated that β-actin with MTS was localized both around and inside the mitochondria (Figure S5C). We analyzed the MMP by MitoTracker Orange staining and found a significant rescue effect of MMP only in KO::ActbMTS cells, when compared with KO::GFP cells (Figure 4E). The same results were seen by TMRE staining analysis (Figure S5D). We found that whereas mtDNA copy number remained unchanged between KO::GFP and KO::ActbMTS (Figure 4F), an increase in the transcript from mtDNA was detected in KO::ActbMTS cells (Figure 4G), suggesting that mitochondrial β-actin can directly regulate mtDNA transcription. Interestingly, upon the expression of ActbMTS we also found a tendency in the up-regulation of nuclear OXPHOS genes (Figure S5E), which further implies a cross talk between mtDNA expression and nuclear transcription of OXPHOS genes.

DISCUSSION

Our study provides novel and direct evidence supporting the functional localization of β-actin inside mitochondria. Although early studies reported the possible presence of actin in mitochondria, its presence was questioned due to the lack of an MTS in the actin protein and the high potential for contamination in isolated mitochondria (Etoh et al., 1990; Lo et al., 2003). In line with previous observation, our results show the presence of β-actin within mammalian mitochondria and reveal that network-like β-actin structures are interconnected between the cytosol and mitochondria. Recent evidence strongly support the presence of actin in human mitochondria and its tight association with mtDNA (Reyes et al., 2011). It remains to be established whether this association is direct or indirect, occurring through intermediate proteins (Boldogh et al., 2003; Hobbs et al., 2001). Interestingly, in plant cells, electron microscopy with immunogold labeling showed that actin resides in the mitochondrial matrix (Lo et al., 2011). A recent quantitative proteomic analysis of yeast mitochondria also identified yeast actin (ACT1) as a component of mitochondria with high confidence (Morgenstern et al., 2017). Together, these studies also support the presence of actin in the mitochondria of different organisms.

As β-actin and myosin associate with mtDNA (Reyes et al., 2011), it is likely this interconnected actomyosin network functions to support proper mtDNA replication, thereby regulating mtDNA copy number. Interestingly, previous studies reported that actin can be co-purified with mitochondrial nucleoid factors such as TFAM and mitochondrial transcription termination factor 2 (MTERF2) (Kanki et al., 2004; Pellegrini et al., 2009). We observed that in the absence of β-actin-containing network in mitochondria of KO cells, TFAM-based nucleoid clustered to large aggregates. Together, β-actin-containing structure may function as a "mitoskeleton" to physically support TFAM-based nucleoid segregation and distribution. Considering that the ancestral prokaryotes utilize actin-like cytoskeleton in the similar process of plasmid partitioning (Carballido-Lopez, 2006), actin-based mechanism seems to be fundamental for circular DNA segregation.

Our data also demonstrate an essential functional role of β-actin in mitochondrial quality control. Importantly, β-actin is indispensable for maintaining mtDNA transcription and MMP. The absence of β-actin impaired OXPHOS activity and cellular ATP level. It is noteworthy that the recently observed up-regulation of other actin isoforms such as smooth muscle α-actin and cytosolic γ-actin in KO cells (Xie et al., 2018) does not functionally compensate for the loss of β-actin in mitochondrial quality control. In addition, only β-actin but not γ-actin was identified in isolated mtDNA (Reyes et al., 2011), suggesting that the role in maintaining mtDNA transcription, mtDNA copy number, and MMP is specific for β-actin. It is most likely that the lack of mitochondrial pool of β-actin accounts for the mtDNA transcription defects observed in β-actin-null cells because only mitochondria-targeted β-actin shows rescue effects on mtDNA transcription and MMP. In the cell nucleus, β-actin, together with actin-binding proteins, is involved in transcription regulation and chromatin remodeling (Virtanen and Vartiainen, 2017; Visa and Percipalle, 2010). Since mitochondria have their own transcription apparatus, it is plausible to speculate that β-actin interacts with mtDNA-binding proteins to regulate nucleoid topology and affects mtDNA transcription. Further studies are required to address the potential involvement of myosin in mtDNA transcription.

The transcription of nuclear OXPHOS genes seems to be correlated with mtDNA transcription. Without β-actin, mtDNA expression is impaired and nuclear OXPHOS genes are down-regulated. The expression of nuclear OXPHOS genes tend to increase when mitochondria-targeted β-actin is re-introduced to boost mtDNA transcription. Several mito-nuclear communication pathways have been found in both anterograde and retrograde manners under stress conditions and proteostasis regulation (Quiros et al., 2016; Ryan and Hoogenraad, 2007). Although it has been noted that the expression of mtDNA and nuclear OXPHOS genes are correlated (Gagnon et al., 1991), the molecular players mediating the coordination remain to be identified.

One open question is how β-actin is imported into mitochondria. Owing to the unique double membrane structure of mitochondria, mitochondria relies on specialized protein translocases for protein import (Dudek et al., 2013). However, cytosolic proteins can be imported into organelles via uncanonical routes (Lo et al., 2011). Interestingly, a study by Reyes et al. (2011) shows that import of β-actin into isolated mitochondria seems to be dependent on the proton gradient, suggesting an undiscovered route of protein import by mitochondria.

In conclusion, our study unveils a previously unknown role of β-actin inside mitochondria. β-Actin-containing structures inside mitochondria are required for optimal mtDNA transcription and MMP maintenance.

METHODS

All methods can be found in the accompanying Transparent Methods supplemental file.

SUPPLEMENTAL INFORMATION

Supplemental Information includes Transparent Methods, five figures, and three videos and can be found with this article online at https://doi.org/10.1016/j.isci.2018.04.021.

AUTHOR CONTRIBUTIONS

X.X. and P.P. designed research; X.X. and T.V. performed experiments; X.X., T.V., N.D., and P.P. analyzed the data; and X.X., P.P. wrote the paper. All authors read and approved the final manuscript.

DECLARATION OF INTERESTS

The authors declare no conflict of interest.

REFERENCES

Boldogh, I.R., Nowakowski, D.W., Yang, H.C., Chung, H., Karmon, S., Royes, P., and Pon, L.A. (2003). A protein complex containing Mdm10p, Mdm12p, and Mmm1p links mitochondrial membranes and DNA to the cytoskeleton-based segregation machinery. Mol. Biol. Cell *14*, 4618–4627.

Boldogh, I.R., and Pon, L.A. (2006). Interactions of mitochondria with the actin cytoskeleton. Biochim. Biophys. Acta *1763*, 450–462.

Carballido-Lopez, R. (2006). The bacterial actin-like cytoskeleton. Microbiol. Mol. Biol. Rev. *70*, 888–909.

Chatterjee, A., Seyfferth, J., Lucci, J., Gilsbach, R., Preissl, S., Bottinger, L., Martensson, C.U., Panhale, A., Stehle, T., Kretz, O., et al. (2016). MOF Acetyl transferase regulates transcription and respiration in mitochondria. Cell *167*, 722–738.

Clejan, L., Bosch, C.G., and Beattie, D.S. (1984). Inhibition by dicyclohexylcarbodiimide of proton ejection but not electron-transfer in rat-liver mitochondria. J. Biol. Chem. *259*, 3017–3020.

Dominguez, R., and Holmes, K.C. (2011). Actin structure and function. Annu. Rev. Biophys. *40*, 169–186.

Dudek, J., Rehling, P., and van der Laan, M. (2013). Mitochondrial protein import: common principles and physiological networks. Biochim. Biophys. Acta *1833*, 274–285.

Dzbek, J., and Korzeniewski, B. (2008). Control over the contribution of the mitochondrial membrane potential (DeltaPsi) and proton gradient (DeltapH) to the protonmotive force (Deltap). In silico studies. J. Biol. Chem. *283*, 33232–33239.

Etoh, S., Matsui, H., Tokuda, M., Itano, T., Nakamura, M., and Hatase, O. (1990). Purification and immunohistochemical study of actin in mitochondrial matrix. Biochem. Int. *20*, 599–606.

Gagnon, J., Kurowski, T.T., Wiesner, R.J., and Zak, R. (1991). Correlations between a nuclear and a mitochondrial messenger-RNA of cytochrome-C-oxidase subunits, enzymatic-activity and total messenger-Rna content, in rat-tissues. Mol. Cell. Biochem. *107*, 21–29.

Gourlay, C.W., and Ayscough, K.R. (2005). The actin cytoskeleton: a key regulator of apoptosis and ageing? Nat. Rev. Mol. Cell Biol. *6*, 583–589.

Hamon, M.P., Bulteau, A.L., and Friguet, B. (2015). Mitochondrial proteases and protein quality control in ageing and longevity. Ageing Res. Rev. *23*, 56–66.

Hobbs, A.E.A., Srinivasan, M., McCaffery, J.M., and Jensen, R.E. (2001). Mmm1p, a mitochondrial outer membrane protein, is connected to mitochondrial DNA (mtDNA) nucleoids and required for mtDNA stability. J. Cell Biol. *152*, 401–410.

Kanki, T., Nakayama, H., Sasaki, N., Takio, K., Alam, T.I., Hamasaki, N., and Kang, D. (2004). Mitochondrial nucleoid and transcription factor A. Ann. N. Y. Acad. Sci. *1011*, 61–68.

Kruse, T., and Gerdes, K. (2005). Bacterial DNA segregation by the actin-like MreB protein. Trends Cell Biol. *15*, 343–345.

Kukat, C., Davies, K.M., Wurm, C.A., Spahr, H., Bonekamp, N.A., Kuhl, I., Joos, F., Polosa, P.L., Park, C.B., Posse, V., et al. (2015). Cross-strand binding of TFAM to a single mtDNA molecule forms the mitochondrial nucleoid. Proc. Natl. Acad. Sci. USA *112*, 11288–11293.

Kukat, C., and Larsson, N-G. (2013). mtDNA makes a U-turn for the mitochondrial nucleoid. Trends Cell Biol. *23*, 457–463.

Kukat, C., Wurm, C.A., Spahr, H., Falkenberg, M., Larsson, N-G., and Jakobs, S. (2011). Super-resolution microscopy reveals that mammalian mitochondrial nucleoids have a uniform size and frequently contain a single copy of mtDNA. Proc. Natl. Acad. Sci. USA *108*, 13534–13539.

Leonard, A.P., Cameron, R.B., Speiser, J.L., Wolf, B.J., Peterson, Y.K., Schnellmann, R.G., Beeson, C.C., and Rohrer, B. (2015). Quantitative analysis of mitochondrial morphology and membrane potential in living cells using high-content

imaging, machine learning, and morphological binning. Biochim. Biophys. Acta *1853*, 348–360.

Lo, Y.S., Cheng, N., Hsiao, L.J., Annamalai, A., Jauh, G.Y., Wen, T.N., Dai, H., and Chiang, K.S. (2011). Actin in mung bean mitochondria and implications for its function. Plant Cell *23*, 3727–3744.

Lo, Y.S., Wang, Y.T., Jane, W.N., Hsiao, L.J., Chen, L.F.O., and Dai, H. (2003). The presence of actin-like protein filaments in higher plant mitochondria. Bot. Bull. Acad. Sinica *44*, 19–24.

Moller-Jensen, J., Jensen, R.B., Lowe, J., and Gerdes, K. (2002). Prokaryotic DNA segregation by an actin-like filament. EMBO J. *21*, 3119–3127.

Morgenstern, M., Stiller, S.B., Lübbert, P., Peikert, C.D., Dannenmaier, S., Drepper, F., Weill, U., Höß, P., Feuerstein, R., Gebert, M., et al. (2017). Definition of a high-confidence mitochondrial proteome at quantitative scale. Cell Rep. *19*, 2836–2852.

Murdock, D.G., Boone, B.E., Esposito, L.A., and Wallace, D.C. (1999). Up-regulation of nuclear and mitochondrial genes in the skeletal muscle of mice lacking the heart/muscle isoform of the adenine nucleotide translocator. J. Biol. Chem. *274*, 14429–14433.

Pellegrini, M., Asin-Cayuela, J., Erdjument-Bromage, H., Tempst, P., Larsson, N.G., and Gustafsson, C.M. (2009). MTERF2 is a nucleoid component in mammalian mitochondria. Biochim. Biophys. Acta *1787*, 294–302.

Qi, X., Qvit, N., Su, Y.C., and Mochly-Rosen, D. (2013). A novel Drp1 inhibitor diminishes aberrant mitochondrial fission and neurotoxicity. J. Cell Sci. *126*, 789–802.

Quiros, P.M., Mottis, A., and Auwerx, J. (2016). Mitonuclear communication in homeostasis and stress. Nat. Rev. Mol. Cell Biol. *17*, 213–226.

Reyes, A., He, J., Mao, C.C., Bailey, L.J., Di Re, M., Sembongi, H., Kazak, L., Dzionek, K., Holmes, J.B., Cluett, T.J., et al. (2011). Actin and myosin contribute to mammalian mitochondrial DNA maintenance. Nucleic Acids Res. *39*, 5098–5108.

Ryan, M.T., and Hoogenraad, N.J. (2007). Mitochondrial-nuclear communications. Annu. Rev. Biochem. *76*, 701–722.

Safiulina, D., Veksler, V., Zharkovsky, A., and Kaasik, A. (2006). Loss of mitochondrial membrane potential is associated with increase in mitochondrial volume: physiological role in neurones. J. Cell. Physiol. *206*, 347–353.

Schieke, S.M., Phillips, D., McCoy, J.P., Jr., Aponte, A.M., Shen, R.F., Balaban, R.S., and Finkel, T. (2006). The mammalian target of rapamycin (mTOR) pathway regulates mitochondrial oxygen consumption and oxidative capacity. J. Biol. Chem. *281*, 27643–27652.

Senning, E.N., and Marcus, A.H. (2010). Actin polymerization driven mitochondrial transport in mating *S. cerevisiae*. Proc. Natl. Acad. Sci. USA *107*, 721–725.

Sharili, A.S., Kenny, F.N., Vartiainen, M.K., and Connelly, J.T. (2016). Nuclear actin modulates cell motility via transcriptional regulation of adhesive and cytoskeletal genes. Sci. Rep. *6*, 33893.

Shestakova, E.A., Singer, R.H., and Condeelis, J. (2001). The physiological significance of beta-actin mRNA localization in determining cell polarity and directional motility. Proc. Natl. Acad. Sci. USA *98*, 7045–7050.

Toei, M., and Noji, H. (2013). Single-molecule analysis of F0F1-ATP synthase inhibited by N,N-dicyclohexylcarbodiimide. J. Biol. Chem. *288*, 25717–25726.

Tondeleir, D., Lambrechts, A., Muller, M., Jonckheere, V., Doll, T., Vandamme, D., Bakkali, K., Waterschoot, D., Lemaistre, M., Debeir, O., et al. (2012). Cells lacking beta-actin are genetically reprogrammed and maintain conditional migratory capacity. Mol. Cell. Proteomics *11*, 255–271.

van Waveren, C., and Moraes, C.T. (2008). Transcriptional co-expression and co-regulation of genes coding for components of the oxidative phosphorylation system. BMC Genomics *9*, 18.

Virtanen, J.A., and Vartiainen, M.K. (2017). Diverse functions for different forms of nuclear actin. Curr. Opin. Cell Biol. *46*, 33–38.

Visa, N., and Percipalle, P. (2010). Nuclear functions of actin. Cold Spring Harb. Perspect. Biol. *2*, a000620.

Wang, Y., and Bogenhagen, D.F. (2006). Human mitochondrial DNA nucleoids are linked to protein folding machinery and metabolic enzymes at the mitochondrial inner membrane. J. Biol. Chem. *281*, 25791–25802.

Xie, X., Stubbington, M.J., Nissen, J.K., Andersen, K.G., Hebenstreit, D., Teichmann, S.A., and Betz, A.G. (2015). The regulatory T cell lineage factor Foxp3 regulates gene expression through several distinct mechanisms mostly independent of direct DNA binding. PLoS Genet. *11*, e1005251.

Xie, X., Almuzzaini, B., Drou, N., Kremb, S., Yousif, A., Farrants, A.O., Gunsalus, K., and Percipalle, P. (2018). β-actin dependent global chromatin organization and gene expression programs control cellular identity. FASEB J. *32*, 1296–1314.
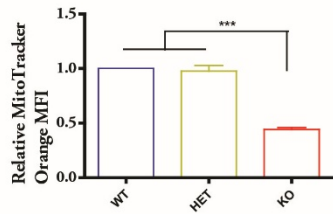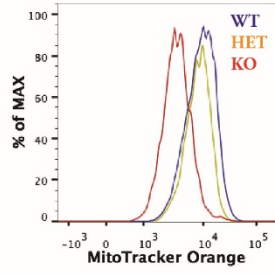
Supplemental Information

In Mitochondria β-Actin Regulates

mtDNA Transcription and Is Required

for Mitochondrial Quality Control

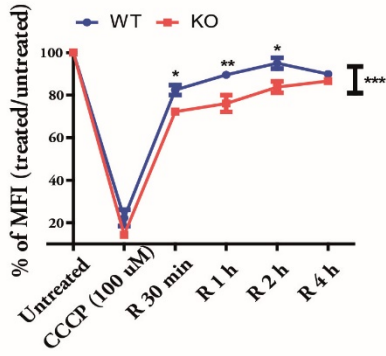Xin Xie, Tomas Venit, Nizar Drou, and Piergiorgio Percipalle
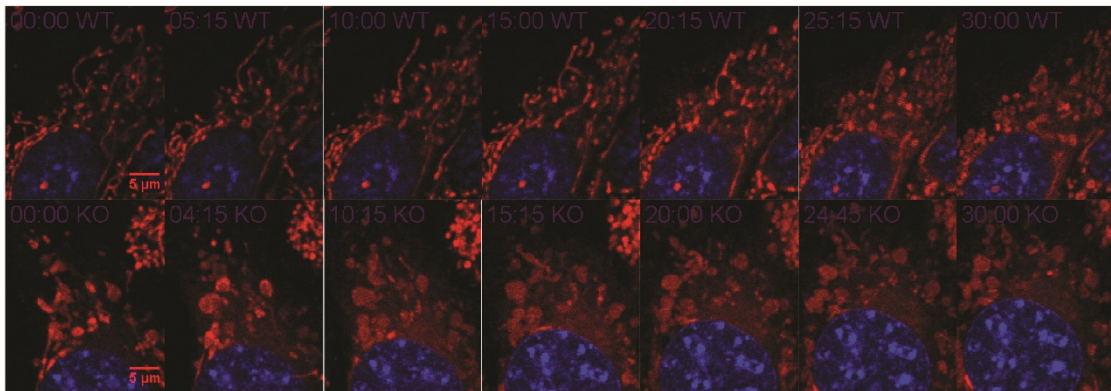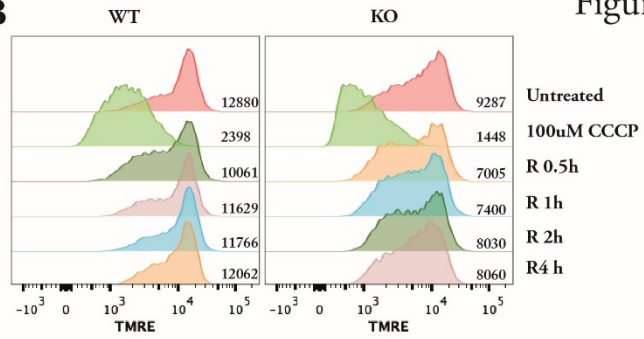
Supplemental Figures and Legends

Figure S1

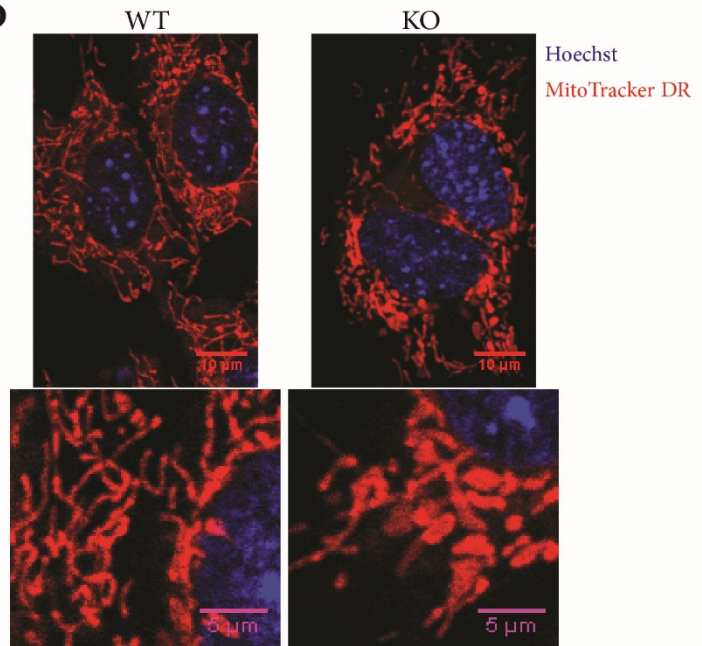**Figure S1. Impaired ability to maintain MMP and altered mitochondira morphology in β-actin null MEFs, related to Figure 1.**

(A) FACS analysis of MMP in WT (β-actin+/+), HET (β-actin+/-) and KO (β-actin-/-) MEFs, stained by MitoTracker Orange (n=3). One-way ANOVA: ***: $p<0.001$, Mean ± S.E.M.

(B-C) WT and KO MEFs were depolarized by 100 µM CCCP for 2 h. Then CCCP-contained medium was replaced with fresh medium. The MMP changes at each time point was determined by TMRE staining in (B). The mean TMRE fluorescence intensity of untreated WT and KO cells were set as 100 and the MMP at each time point was normalized to untreated sample in (C). Data are summary of 3 biological replicates. Two-way ANOVA: *: $p<0.05$; **: $p<0.01$; ***: $p<0.001$. Mean ± S.E.M.

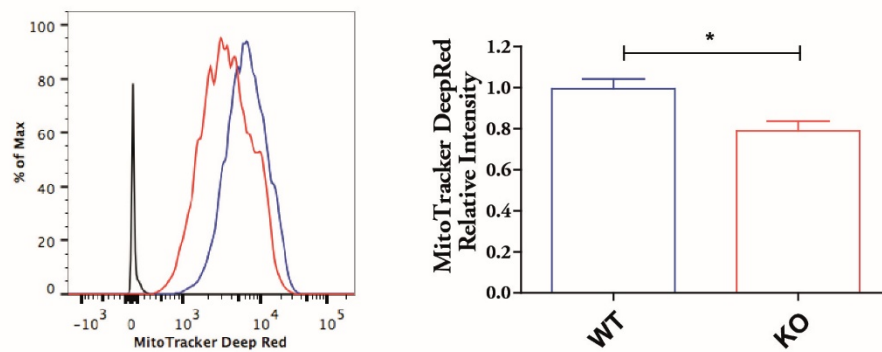(D) Confocal images of live cell mitochondria staining by MitoTracker Deep Red.

(E) Live cells stained with MitoTracker Deep Red were treated with MPP+. A serious of confocal images were taken immediately after MPP+ addition. The corresponding time points of each image were shown on the top left.

A

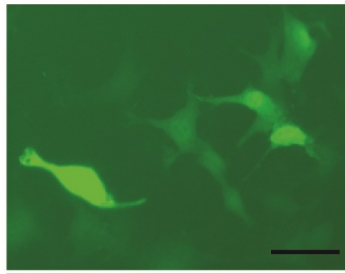|	
KO Chromosome 9	[0 - 5.00]
WT Chromosome 9	[0 - 5.00]
KO mtDNA	[0 - 110]
WT mtDNA	[0 - 110]
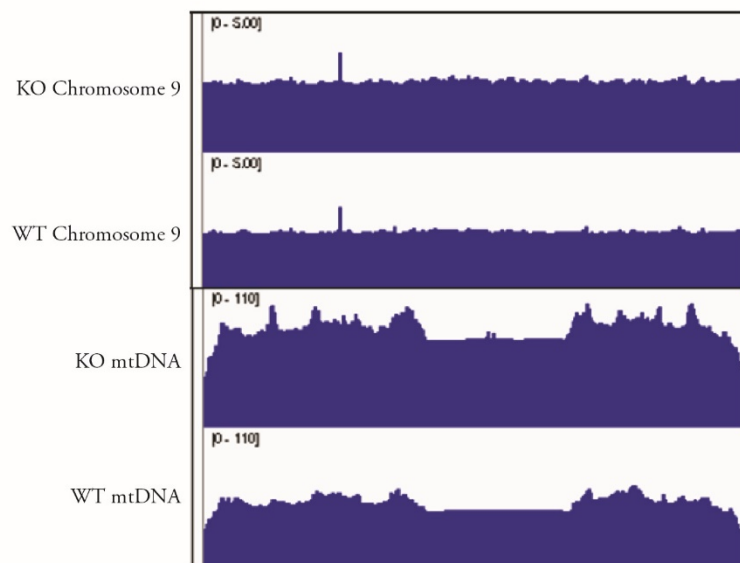
B

Figure S2. Increased mtDNA copy number but reduced mitochondrial mass in KO cells, related to Figure 2.
(A) Total DNA isolated from cells were subjected to DNA sequencing. Normalized sequencing reads shows the relatively higher level of mtDNA in KO cells when compared to WT cells, while the nuclear reads level are the same between WT and KO cells.
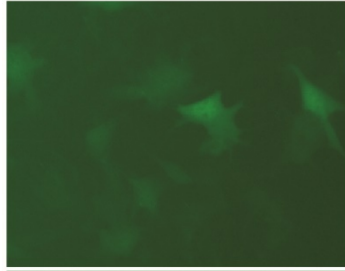(B) FACS estimate of mitochondrial mass by MitoTracker Deep Red staining. Mean fluorescence intensity (MFI) of MitoTracker Deep Red staining was summarized from 3 biological replicates. Student's t Test, * $P<0.05$. Mean ± S.E.M.
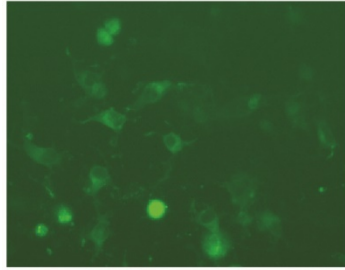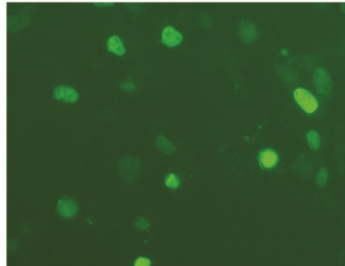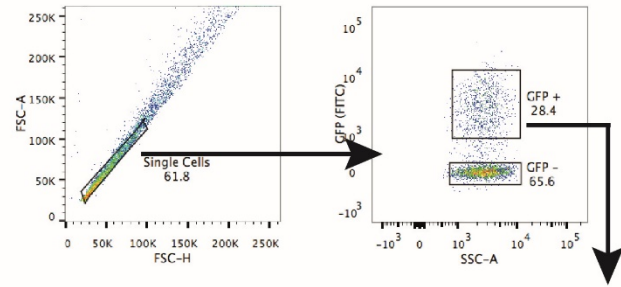
A

WT+GFP

KO+GFP

KO+GFP-Actin

KO+GFP-NLS-Actin

B

Figure S3

Single Cells
61.8

GFP +
28.4

GFP –
65.6

C

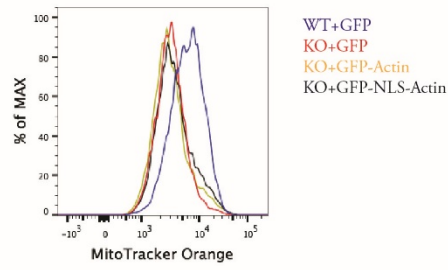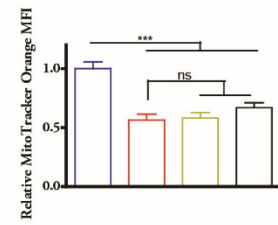WT+GFP
KO+GFP
KO+GFP-Actin
KO+GFP-NLS-Actin

D

ns

***

E

WT murine Actb, KO human Actb
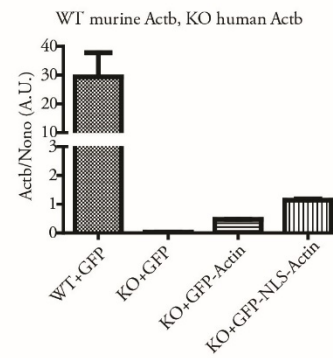
Figure S3. Transient expression of actin or NLS-targeted actin failed to rescue MMP in KO cells, related to Figure 3.

(A) Images showing the distribution of GFP signal in GFP, GFP-actin and GFP-NLS-Actin transfected cells.

(B-D) Cells were transfected with GFP, GFP-actin and GFP-NLS-Actin construct. 48 h post-transfection, cells were stained with MitoTracker Orange and analyzed by FACS. (B). Gating of GFP+ cells were shown. (C). Overlaid histograms showing GFP+ population of each samples in terms of the MitoTracker Orange staining intensity. (D). Relative of MitoTracker Orange MFI, data are summary of 3 biological replicates, representative of 2 independent experiment. One-way ANOVA: ***: $p<0.001$. Mean ± S.E.M.

(E) Relative β-actin mRNA levels. In WT and KO cells with GFP, endogenous β-actin was determined using primer specific for murine β-actin. In KO+GFP-Actin and KO+GFP-NLS-Actin cells, introduced β-actin from human origin was determined using primer specific for human β-actin. Data were normalized to endogenous *Nono* gene. Data show the triplicate measurement of sorted GFP+ cells. Mean ± S.E.M.

Figure S4

A

Phalloidin
MitoTracker DR

B

Merge   Phalloidin   MitoTracker DR
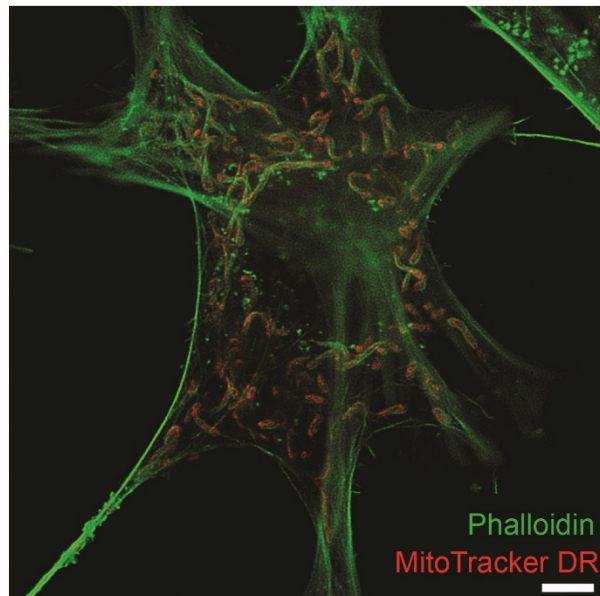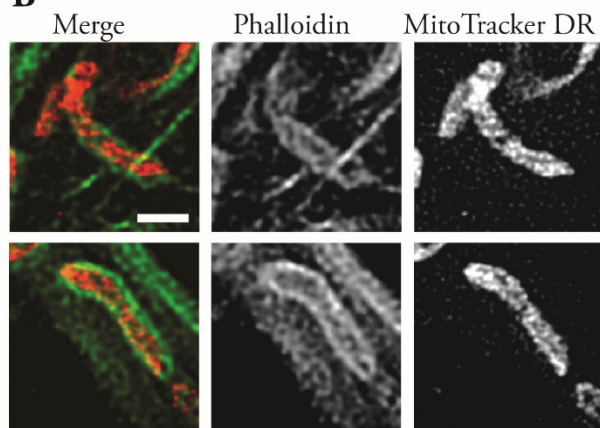
C TFAM ChIP-seq on Mitochondrial genome

Mitochondrial DNA 16 kb

WT ChIP1
WT ChIP2
KO ChIP1
KO ChIP2
WT Input 1
KO Input 1

7
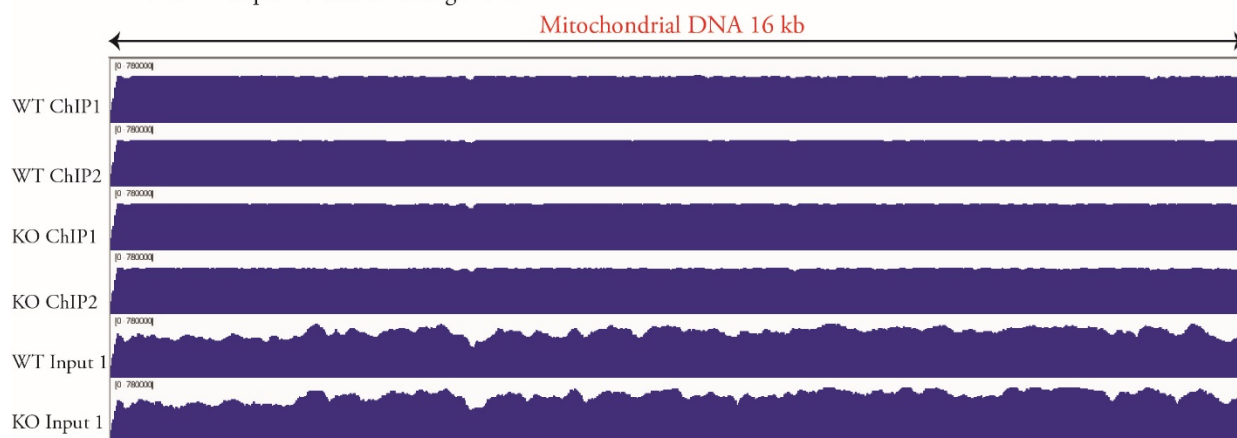
Figure S4. Super-resolution image of Mitochondria and Phalloidin co-staining, related to Figure 3.

(A) WT MEFs were stained with MitoTracker Deep Red and Phalloidin-iFluor 555 and visualized using STED microscope. Scale Bar: 5 µM.

(B) Insets from (A) showing the strong phalloidin staining surrounding mitochondria and weak phalloidin staining within mitochondria. Scale Bar: 1 µM.

(C) TFAM ChIP-seq analysis on mitochondrial genome. Two biological replicates of TFAM ChIP-seq and one input of each cell type was shown. TFAM ChIP-seq signals in WT and KO cells show even distribution across the whole mitochondrial genome. Y-axis of each track shows the value of RPKM (Reads Per Kilobase per Million mapped reads).

A

| HA | GFP | IRES | rat CD8a |

| HA | Actb | IRES | rat CD8a |

| HA | ActbNLS | IRES | rat CD8a |

SV40 NLS: PKKKRKV

| HA | ActbMTS | IRES | rat CD8a |

COX4 mitochondrial targeting signal (MTS): MLATRVFSLVGKRAISTSVCVRAH

Figure S5

B

WT::Untransduced
rCD8a+ 0.052

KO::Untransduced
rCD8a+ 0.013

WT::GFP
rCD8a+ 90.0

KO::GFP
rCD8a+ 88.9

KO::Actb
rCD8a+ 90.5

KO::ActbNLS
rCD8a+ 91.8

KO::ActbMTS
rCD8a+ 90.4

C

KO::ActbMTS

HA staining
MitoTracker DR

Merge   MitoTracker DR   HA

D

WT::GFP
KO::GFP
KO::Actb
KO::ActbNLS
KO::ActbMTS

E

KO::GFP   KO::ActbMTS

$p=0.059$

*

*

9
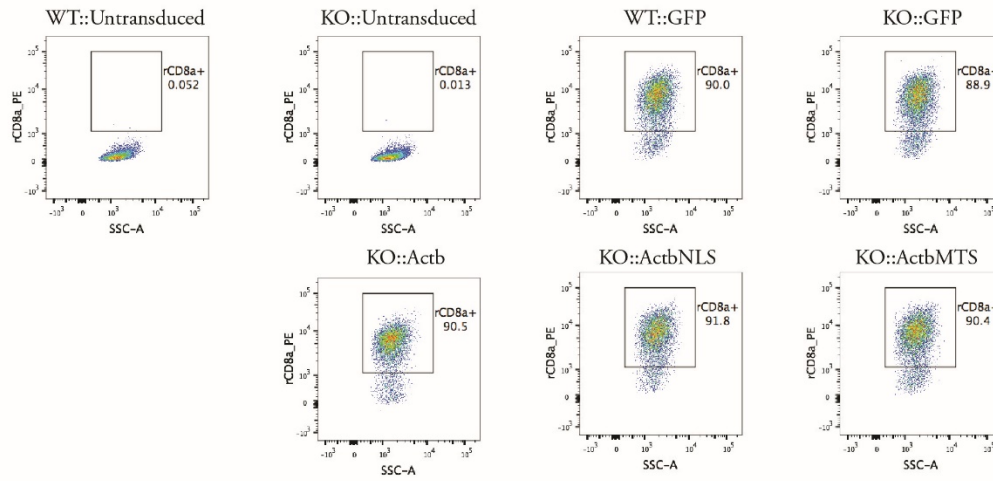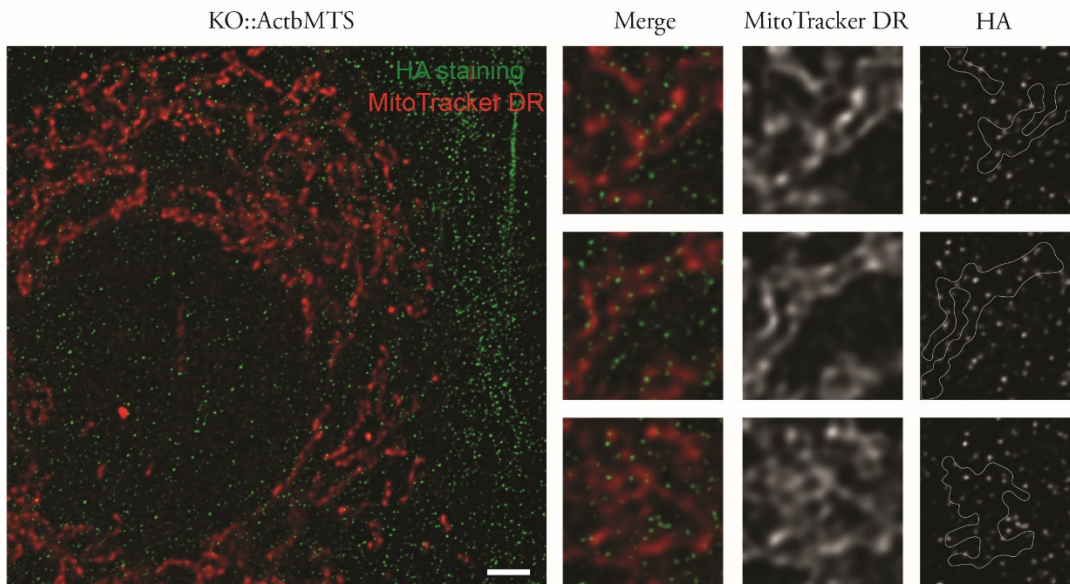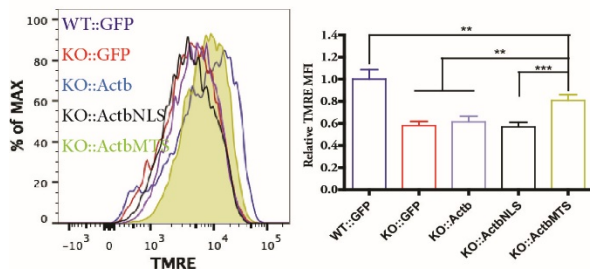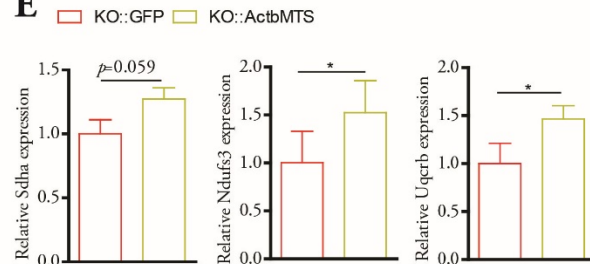
Figure S5. Mitochondria-targeted β-actin partially rescue MMP in KO cells, related to Figure 4.

(A) Schematics of retroviral construct used for reintroducing Actb gene, Actb with SV40 NLS (nucleus localization signal) or Actb with Cox4 MTS (mitochondrial targeting signal) into KO cells. rCD8a was co-expressed as a surface marker for sorting. GFP was used as control.

(B) Cells transduced with corresponding virus (e.g. KO::GFP, KO cells transduced with virus carrying GFP). Transduced cells were stained with anti-rCD8a-PE antibody and sorted for PE+ population. Dot plots show the percentage of rCD8a+ cells after sorting and cell expansion.

(C) STED microscope image showing the localization of HA-tagged β-actin with MTS (ActbMTS) inside mitochondria. Scale bar: 3 µm. Several insets of MitoTracker DR and HA staining examples were shown in right panel.

(D) Cells in were stained with TMRE and analyzed by FACS. The relative mean TMRE fluorescence intensity were shown in histogram. Data is the summary of 3 independent experiments. One-way ANOVA: **: $p<0.01$, ***: $p<0.001$. Mean ± S.E.M.

(E) qPCR quantification of relative nuclear OXPHOS genes expression in KO::GFP and KO::ActbMTS cells. Data is the summary of 3 independent experiments. Student's t test: *: $p<0.05$. Mean ± S.E.M.

Transparent Methods

Antibodies and reagents:

Antibody of HA (ab9110) and Phalloidin-iFluor 555 reagent was from Abcam. Antibody against β-actin (clone AC-74), Carbonyl cyanide 3-chlorophenylhydrazone (CCCP, C2759), MPP$^+$ iodide (D048), Tetramethylrhodamine ethyl ester perchlorate (TMRE, 87917), Rotenone (R8875), 2-Thenoyltrifluoroacetone (TTFA, T27006), Antimycin A (A8674), Potassium cyanide (KCN, 60178), N,N′-Dicyclohexylcarbodiimide (DCCD, 36650), polybrene (H9268), DMEM medium high glucose (D5671), Fetal Bovine Serum (F0804), Penicillin-Streptomycin (P0781), 2X Laemmli Sample buffer (S3401) were from Sigma-Aldrich. Antibodies of mouse IgG Dylight 550 (84540), rabbit IgG Dylight 550 (84541), MitoTracker™ Orange CMTMRos (M7510), MitoTracker™ Deep Red FM (M22426), Hoechst 43222 (H1399), Click-iT™ Nascent RNA Capture Kit (C10365), Maxima SYBR Green qPCR Master Mix (K0252), RevertAid First Strand cDNA Synthesis Kit (K1622), DNA-free™ DNA Removal Kit (AM1906), Mitochondria Isolation Kit (89874), Pierce™ ECL Western Blotting Substrate (32106), Pierce™ Protein Assay Kit (23225), ATP Determination Kit (A22066), PureLink Genomic DNA Mini Kit (K182001), TRIzol® Reagent (15596-018) and Lipofectamine™ 3000 Transfection Reagent (L3000015) were purchased from Thermo Fisher Scientific. Anti-rat CD8a-PE (201706) antibody was purchased from Biolegend. Anti-GAPDH-HRP (HRP-60004) was from ProSci. MitoCheck® Complex II/III Activity Assay Kit (700950) was from Cayman Chemical. Qiaquick PCR Purification Kit (28106) and RNeasy Mini Kit (74106) were purchased from Qiagen. Anti-TFAM (ABE483) and Magna ChIP Protein A+G Magnetic Beads (16-663) were from Merk Millipore. The concentration of the compounds and dilution of antibodies are indicated in each experiment respectively.

Cell culture:

The β-actin$^{+/+}$ MEFs (WT), β-actin$^{+/-}$ MEFs (HET) and β-actin$^{-/-}$ MEFs (KO), and mouse endothelial cell line C166 (ATCC) were maintained and cultured with Dulbecco's modified Eagle medium (DMEM) with high glucose (Sigma), 10% fetal bovine serum (Sigma) and 100 units/mL penicillin and 100 μg/mL streptomycin (Sigma), in a humidified incubator with 5% CO^2 at 37 ºC.

Mitochondrial analysis using high-content screening (HCS) Platform:

MEFs were cultured in 96-well back, clear bottom plate (Corning), at density of 5000 cells/well. After 24 h culture, cells were stained with 100 nM MitoTracker Orange CMTMRos for 20 min. Stained cells were washed twice with PBS and fixed by 3.7% formaldehyde for 15 min. After 2 times PBS wash, cells were further stained with Hoechst 43222 (1:6000) for 15 min. After 2 times wash with PBS, stained cells in plate were scanned via Cellomics ArrayScan™ XTI High Content Analysis (HCS) platform (Thermo Fisher Scientific), with a 20x Objective. Compartment Analysis Bio Application software (Cellomics) was applied to quantitatively analyze the MitoTracker staining spots in the simulated cytoplasm of individual cells based on nuclear Hoechst staining. For each experiment, at least 500 valid single cells per culture well were quantified and at least 10 independent culture wells (10 biological replicates) were analyzed.

Flow cytometry analysis:

To compare the membrane potential between WT and KO cells, cells at 70% confluence in 24 or 6 well plate were incubated with medium containing 100 nM MitoTracker Orange CMTMRos, or 0.2 to 2.0 µM TMRE for 20 min. For the assessment of mitochondrial mass, cells were stained with 200 nM MitoTracker™ Deep Red FM for 30 min. After staining, cells were washed 2 times with PBS. Trypsinized cells were re-suspended in PBS, following by immediate analysis via flow cytometer BD FACSAria III.

For the assessment of chemical inhibitors on membrane potential changes, cells were incubated with medium containing CCCP (30 µM), MPP+ (2mM) for 1h, Rotenone (15 µM), TTFA (800 µM) Antimycin A (30 µM), KCN (2 mM) and DCCD (150 µM) for 20 min. Cells with or without treatment were stained with 1 µM TMRE for 20 min. After 2 times washes with PBS, trypsinized cells were re-suspended in PBS and immediately analyzed by flow cytometer BD FACSAria III.

For the analysis of mitochondrial membrane potential recovery after CCCP treatment, cells were treated with 100 µM CCCP for 2 h and cells were washes once with fresh medium. Fresh medium was added to allow the cells to recover from CCCP-induced membrane potential loss. Cells at different time points of recovery were stained with 1 µM TMRE for 20 min and then analyzed by FACS.

For all samples, at least 10,000 cell events were recorded. Data from flow cytometer BD FACSAria III were analyzed using Flow Jo software.

RNA-Seq analysis:

Total RNA was extracted from 70% confluent cells using TRI Reagent according to the manufacturer protocol (Sigma-Aldrich). Quality of total RNA were evaluated at SciLIfe lab (Stockholm, Sweden) using Qubit and Bioanalyzer respectively. 1 µg total RNA of Samples that passed the QC assessment were used for library construction using TruSeq Stranded mRNA Library Prep Kit (Illumina) according to the manufacturer protocol. Deep sequencing was performed at SciLife Laboratory, the National Genomics Infrastructure, NGI, Karolinska Institute, Stockholm. Illumina HiSeq 2000 sequencer was used to produce 50 bp single-end reads, following manufacturers' protocols.

The sequencing data was processed through the standard RNAseq analysis pipeline at NYUAD. Sequenced reads were trimmed for adaptor sequence, and masked for low-complexity or low-quality sequence, then mapped to the Mus musculus GRCm38.p4 genome using tophat2 v2.1.0 with the parameters "–no-novel-junctions" and "–G" when specifying the genome file. Cufflinks v2.2.1 was used to derive FPKM (Fragments Per Kilobase of transcript per Million mapped reads). Differential gene expression was analyzed by Cuffdiff. RNA-seq data was deposited in GEO repository and the GEO accession number is GSE95830.

Immunofluorescence, live cell imaging and super-resolution microscopy:

Cells grown on glass cover slip were stained with 100 nM MitoTracker Orange CMTMRos, or 200 nM MitoTracker™ Deep Red FM for 20 min. Stained cells were then washed 2 times with fresh medium and then cultured in fresh medium for 1 h before being fixed by 70% cold ethanol for antibody staining. For phalloidin staining, cells were fixed with 4% formaldehyde. Fixed cells were permeabilized with 0.5% Triton X-100 in PBS for 15 min. After blocking by 1% BSA for 1 h, cells were stained with primary antibodies against HA (1:200), TFAM (1:200) or β-actin (1:150), or Phalloidin iFluor 555 reagent (1:1000) for 2 h. The cells were washed 3 times with TBST buffer. The antibody-stained cells further stained with corresponding dylight 550-conjugated secondary antibody (1:1000) and Hoechst 43222 (1:6000) for 1 h. The cover slip was mounted to glass slide using Molecular Probes ProLong® Gold anti-fade mounting media (Invitrogen). Stained cells were observed using Olympus FV1000 confocal microscope.

For live cell imaging of mitochondria, cells grown on glass-bottom CELLview culture dish (Greiner Bio One) were stained with 200 nM MitoTracker™ Deep Red FM for 20 min. After 2 times washes with fresh medium, cells were cultured in incubator for 2 h before imaging. Imaging of mitochondria was performed in a temperature and CO^2 controlled chamber that is connected with Olympus FV1000 confocal microscope system. A time series of confocal images of untreated cells or cells immediately after treatment were captured. Confocal images were captured with 63× immersion oil objective lens, NA 1.4 and a LAS AF software.

Super-resolution images were acquired using Leica TCS SP8 STED 3X microscope equipped with HyD SMD2 detector and Leica HCPL APO CS2 100x/1.51 oil objective. Software Leica application SuiteX was used for capturing and analysis of the images. Huygens Professional software was used for deconvolution. Final data were analyzed and processed by using Fiji software.

TFAM ChIP-seq and analysis:

For TFAM ChIP-seq, chromatin cross-linked *in vivo* by 1% formaldehyde was quenched by 0.125 M Glycine and fragmented using S220 Focused-ultrasonicator (Covaris). 50 ug total fragmented chromatin were mixed with 7 ug anti-TFAM (ABE483) antibody overnight with rotation at 4 Cº. The chromatin-antibody complex were then precipitated with Magna ChIP protein A/G magnetic beads. After washes with low salt wash buffer (20 mM Tris, 2 mM EDTA, 50 mM NaCl, 0.01% SDS and 1% SDS), high salt wash buffer (same composition, 250 mM NaCl) and LiCL-wash buffer (10 mM Tris, 1 mM EDTA, 250 mM LiCl, 1% NP40 and 1% sodium deoxycholate), precipitated chromatin was eluted in 200 µL of elution buffer (10 µL 20% SDS, 20 µL 1M NaHCO$_3$ and 170 µL dH$_2$O).

Reverse cross-linking was done by adding 8 uL 5M NaCl into the eluted solution, with overnight incubation at 65 Cº. After reversing the cross-linking, 1 uL 10 mg/ml RNase A was added, with

30 min incubation at 37°C. Then 4 µL 0.5 M EDTA, 8 µL 1M Tris-HCl and 1 µL 20 mg/mL Proteinase K was added to digest the proteins for 2h at 42°C. The released DNA was purified using QIAquick PCR purification kit (Qiagen). Two biological replicates of ChIP-purified DNA and fragmented total DNA, were used for library preparation using TruSeq Nano DNA Library Prep Kit (Illumina). Deep-sequencing was performed using Illumina HiSEq 2500 sequencing platform to generate 100 bp pair-end reads (New York University Abu Dhabi Sequencing Center).

ChIP-seq data were deposited in GEO database: accession number GSE109532. For analysis, the raw reads were quality-trimmed using Trimmomatic package, and aligned to mitochondrial genome based on mouse reference genome (GRCm38.p4) using Burrows-Wheeler Aligner BWA-MEM 9. Picard tools was used to clean, sort and deduplicate the aligned reads. The processed alignments were normalized in RPKM (reads per kilobase per million mapped reads) with DeepTools2 bamCoverage function.

Western Blotting:

Cell lysate was collected by lysing cells in RIPA buffer and protein concentration was determined by BCA protein assay kit (Thermo Fisher Scientific). Samples were mixed with 2X Laemmli Sample buffer (Sigma) and heated at 95 °C for 5 min. Immunoblotting was performed using anti-HA (1:1000), anti-GAPDH-HRP (1:1000) and goat anti-rabbit IgG HRP (1:2500) antibodies. Protein bands were developed using Pierce ECL western blotting substrate (Thermo Fisher Sceintific), and analyzed by ChemiDoc MP Imaging system (Bio-Rad).

RNA isolation and qPCR:

Total RNA was extracted using RNeasy Mini Kit (Qiagen) according to the manufacturer's instruction. This is followed by DNA removal with DNA-free™ DNA Removal Kit (Themo Fisher Scientific). 500 ng to 1 µg DNase-treated RNA was then reverse transcribed to cDNA using RevertAid First Strand cDNA synthesis Kit (Thermo Fisher Scientific). Quantitative real-time PCR was performed using Maxima SYBR Green qPCR Mix (Thermo Fisher Scientific) on Stratagene 3005 qPCR system (Agilent Technology). All the target gene expression level was normalized to the expression of *Nono* reference gene. Primers of qPCR was listed below:

Gene	Forward primer: 5' – 3'	Reverse primer: 5' – 3'
Actb	TATCGCTGCGCTGGTCG	CCCACGATGGAGGGGAATAC
12S rRNA	TGGTAAATTTCGTGCCAGCCA	AGTTGACACGTTTTACGCCGA
MT-CO1	TTGCAACCCTACACGGAGGT	TCCGGTTAGACCACCAACTGT
MT-ND1	TCGACCTGACAGAAGGAGAATCA	GGGCCGGCTGCGTATT
MT-CYB	AGACAAAGCCACCTTGACCC	GATTGCTAGGGCCGCGATAA
SDHA	GGAACACTCCAAAAACAGACCT	CCACCACTGGGTATTGAGTAGAA
NDUFS3	TGGCAGCACGTAAGAAGGG	CTTGGGTAAGATTTCAGCCACAT
UQCRB	GGCCGATCTGCTGTTTCAG	CATCTCGCATTAACCCCAGTT
Nono	GCCAGAATGAAGGCTTGACTAT	TATCAGGGGGAAGATTGCCCA

RNA synthesis and decay experiment:

Click-iT® Nascent RNA Capture Kit (Thermo Fisher Scientific) was used in this experiment according to the manufacturer's protocol, with some modifications. MEFs cells were tagged with 0.15 mM 5-Ethynyl uridine (EU) as below:

For RNA synthesis analysis, cells were labeled with EU containing growth media for either 2 h (EU 2h) or 4 h (EU 4h). The relative newly synthesized RNA was calculated for 4 h over 2 h pulse labeling duration.

In RNA decay analysis, cells were labeled with EU containing growth media for 2 h (EU 2h). Then cells were washed with fresh culture growth media and cultured for 20 h (EU 2h D20h) in the fresh media without EU.

Total RNA from each sample was harvested using TRIzol® Reagent (Thermo Fisher Scientific). 5 µg total RNA was used in Cu (I) mediated click reaction according to manufacturer's instruction, during which newly synthesized EU-labeled RNA was tagged with biotin. The RNA samples were harvested with TRIzol® Reagent. 150 ng of biotin-tagged RNA were mixed with MYOne T1 Streptavidin magnetic beads to pull down the biotinylated RNA. After sequential washes using Click-iT wash buffer I and wash buffer II, captured RNA on the beads was converted to cDNA by RevertAid First Strand cDNA synthesis Kit (Thermo Fisher Scientific). qPCR quantification was performed in the same manner as described in RNA isolation and qPCR section.

mtDNA copy number quantification:

Total mitochondrial and nuclear genomic DNA was collected using PureLink Genomic DNA Mini Kit (Thermo Fisher Scientific), with protease and RNase treatment according to the manufacturer's instructions. The purified total genomic DNA was quantified by Quantitative real-time PCR, and the mtDNA level was normalized to that of nuclear *Terf* gene. Primers were listed below:

Gene	Forward Primer: 5' – 3'	Reverse primer: 5' – 3'
Terf	CTAGCTCATGTGTCAAGACCCTCTT	GCCAGCACGTTTCTCTCGTT
MT-ND1	ACACTTATTACAACCCAAGAACACAT	TCATATTATGGCTATGGGTCAGG
MT-CYB	AGCCACCTTGACCCGATTCT	CGTGGAGGAAGAGGAGGTGA
MT-ATP6	GCAGTCCGGCTTACAGCTAA	GGTAGCTGTTGGTGGGCTAA

For DNA deep sequencing, total DNA from 1% formaldehyde-fixed MEFs was subject to fragmentation using S220 Focused-ultrasonicator (Covaris). DNA library was prepared by TruSeq Nano DNA Library Prep Kit (Illumina), and then sequenced using Illumina HiSEq 2500 sequencing platform (New York University Abu Dhabi Sequencing Center). The normalized reads (Reads per Kilobase of sequence range per Million mapped reads) were used to compare the relative level of nuclear DNA and mtDNA.

Mitochondrial Complex II/III activity assay:

Mitochondria from 2×10^7 MEFs were purified using Mitochondria Isolation Kit for Cultured Cells (Thermo Fisher Scientific) according to the manufacturer's instruction. The complex II/III activity of freshly isolated mitochondria were determined using MitoCheck® Complex II/III Activity Assay Kit (Cayman Chemical). Briefly, 20 µL mitochondria were mixed with 958 µL Complex III activity assay buffer, 2 µL of 1mM Rotenone and 20 µL of 100 mM KCN as reaction A. Reaction B contains 607 µL Complex III activity assay buffer, 8 µL Succinate reagent and 60 µL Cytochrome c reagent. 50 µL of reaction A was mixed with 20 µL Complex III activity assay buffer and 30 µL reaction B in a 96 well plate. The plate was immediately measured for a kinetic at absorbance 550 nm for 15 min with an interval of 20 seconds at room temperature, using Synergy H1 microplate reader (BioTek). Data was plotted as absorbance (y axis) versus time (x-axis) and the slope of linear portion was the reaction rate, which stands for Complex II/III activity.

ATP determination:

1.5×10^4 MEFs in 96 well plate were lysed with 150 uL NP-40 lysis buffer (150 mM NaCl, 1.0% NP-40 and 50 mM Tris-Cl, pH8.0) on ice for 10 min. After mixing by pipetting up and down, the ATP level was determined using ATP Determination Kit (Thermo Fisher Scientific) according to the manufacturer's instructions. Briefly, reaction solution containing 1X reaction buffer, 1 mM DTT, 0.5 mM D-luciferin, 1.25 µg/mLfirefly luciferase was prepared. 10 µL cell lysate was mixed with 100 µL reaction solution in white 96 well plate and then measured for luminescence via filter set 1 (band pass 528/20) of Synergy H1 microplate reader (BioTek). Blank reaction and standard ATP solution was included as controls.

Cell transfection:

MEFs in 6 well plates were transfected with 3 µg GFP-Actin, GFP-NLS-Actin and M6P-GFP plasmids using Lipofectamine™ 3000 Transfection Reagent (Thermo Fisher Scientific). 48 h post-transfection, the expression of introduced proteins were imaged by EVOS Cell Imaging Systems (Thermo Fisher Scientific) and mitochondria membrane potential was analyzed by FACS.

Retrovirus production and cells transduction:

Retrovirus vector, virus preparation and cell transduction were performed as described previously (Xie et al., 2015). Mouse β-actin open reading frame was cloned from the cDNA of WT MEF and ligated into a retrovector with rCD8a as transduction marker. An SV40 nucleus localization signal (PKKKRKV) or a COX4 mitochondria targeting signal (MLATRVFSLVGKRAISTSVCVRAH) (Chatterjee et al., 2016) was added to the C-terminal of β-actin. Virus supernatant was produced by transfecting 293FT cells in 10 cm dishes with 12 µg of retroviral vector and 12 µg pCL-Eco packaging plasmid (Novus Biologicals) using the Calcium-phosphate precipitation method. Supernatant of transfected 293FT cells was collected at 48 h and 72 h post-transfection and was snap-frozen in liquid nitrogen. For retroviral transduction, MEF cells in 96 well plate were incubated with 100 µL medium and 100 µL viral supernatant, in the presence of 8 µg/mL polybrene. The cell culture were then centrifuged at 2500 rpm for 1.5 h at 32°C to increase the transduction efficiency, and then transferred to incubator. After 12 h incubation, virus-containing medium was

replaced with fresh medium. Cells after expansion were stained with anti-rat CD8a-PE antibody (1:200 in PBS with 5 mM EDTA) for 15 min. Stably transduced rCD8a+ cells were sorted by FACS (BD FACSARIA III) and the sorted cells were further expanded in DMEM with 20% FBS.

Statistics:

All the data values were expressed as means ± SEM. The number of experiments or biological replicates are indicated in the respective figure legends. For direct comparison between two groups, Student's t test was applied. For the comparison of multiple groups, one-way or two-way ANOVA analysis were used, with Tukey's multiple comparison as post hoc test. *P* value less than 0.05 was considered to be statistically significant.